INTERNATIONAL JOURNAL FOR NUMERICAL AND ANALYTICAL METHODS IN GEOMECHANICS
Int. J. Numer. Anal. Meth. Geomech., 2006; **30**:501–527
Published online 28 December 2005 in Wiley InterScience (www.interscience.wiley.com). DOI: 10.1002/nag.490

An analytical study of the effect of penetration rate on piezocone tests in clay

Marcelo F. Silva*,†,‡, David J. White§ and Malcolm D. Bolton¶

Engineering Department, University of Cambridge, U.K.

SUMMARY

Finite element cavity expansion analysis investigating the effect of penetration rate on piezocone tests in clay is presented. A coupled analysis was performed, in which the rate of cavity expansion was linked to the penetration rate of the cone and the cone angle, using the assumption that the deformation was wholly radial, and took place only between the cone tip and the cone shoulder. The soil was modelled using *modified cam* clay with two sets of parameters and varying values of overconsolidation ratio (OCR). The influence of penetration rate on the stress and pore pressure distributions was examined. For slower penetration rates, the excess pore pressure at the cone shoulder is lower since consolidation is permitted coincident with penetration. The radial profiles of post-penetration voids ratio demonstrate that partially drained penetration is permitted by volume change in the near field, in addition to radial movement in the far field. The radial distribution of excess pore pressure after slow penetration differs from the undrained case, with a relatively low radial gradient existing at the cone face. As a result, the dissipation curves after slow penetration lag behind those following fast penetration. The cone velocity is made dimensionless by normalizing with the coefficient of consolidation and the cone diameter. 'Backbone' curves of normalized velocity against normalized tip resistance and excess pore pressure capturing the transition from undrained to drained penetration are derived. The normalized pore pressure backbone curve is unique, whilst the normalized tip resistance shows a small dependency on OCR. These backbone penetration curves are compared with centrifuge model piezocone tests conducted at varying rates, and subsequent dissipation tests. The numerical and experimental results suggest that the value of consolidation coefficient operative during the dissipation phase is 2–4 times higher than the virgin compression value due to changes in the operative soil stiffness, as demonstrated from the stress paths of individual soil elements. The use of multi-rate penetration tests to deduce values of consolidation coefficient is discussed, in light of these differences.

KEY WORDS: piezocone test; rate effect; clay; cavity expansion; dissipation test

*Correspondence to: Marcelo F. Silva, Schofield Centre, High Cross, Madingley Road, Cambridge CB3 0EL, U.K.
†E-mail: mgeot23@gmail.com
‡Research student.
§Lecturer.
¶Professor.

Contract/grant sponsor: CNPq-Brazil
Contract/grant sponsor: Giken Seisakusho Ltd., Kochi, Japan

Received 14 October 2004
Revised 3 August 2005
Accepted 17 August 2005

INTRODUCTION

Since its introduction as an *in situ* investigation device, the piezocone test has provided information which practitioners use to estimate geotechnical parameters. These parameters involve a range of physical and mechanical properties, such as shear strength, deformation, soil state and permeability. Methods for estimating geotechnical parameters from *in situ* test results are more reliable if based on analytical solutions that properly model the penetration process. Investigation of the available methods for the analysis of cone resistance [1] showed that, although various theoretical analyses have been proposed for the penetration process, none is fully rigorous. In practice, most of the parameters have therefore been empirically correlated to the piezocone quantities q_c (cone resistance), f_s (sleeve friction) and u (dynamic pore pressure), for a given case. However, only when the drainage conditions during a piezocone test are fully understood can the combination of the piezocone quantities be correlated to the soil properties.

During insertion, a zone of soil around the piezocone is significantly disturbed. Commonly, this disturbed soil is divided into a plastically deforming region and, at a farther distance, an elastically deforming region. Excluding a region along the piezocone–soil interface in which intense shearing completely remoulds the soil, it is generally accepted that the modes of deformation through which the surrounding soil is subjected during cone penetration are equivalent to the creation of a cavity. It was shown [2] through a combination of strain path and finite element analyses that, for cone angles greater than the standard 60°, the axial plastic boundaries ahead of a piezocone advancing under undrained conditions were comparable with spherical cavity expansion solutions. Recently, Lu *et al.* [3] showed that the radial variation of the direction of computed major principal stresses in the soil surrounding a simulated piezocone also agrees with spherical cavity solutions. Prior to this, Yu and Mitchell [1] had already showed that, in most cases, cavity expansion solutions give the closest agreement between predicted and measured penetration resistance.

Similarly, reviews of analytical methods to describe pore pressure distribution immediately after penetration and during subsequent dissipation in clays [4,5] showed that pore pressure generation can also be adequately predicted by cavity expansion methods (e.g. References [6,7]). These methods compare well with computed analyses from more sophisticated two-dimensional finite element and strain path methods (e.g. References [2,8]). Following penetration, the decay of pore pressure is then mostly predicted on the basis of Terzaghi-Rendulic one-dimensional consolidation theory with radial flow of pore fluid. However, Randolph *et al.* [9] pointed out the inability of these solutions, commonly based on elastic-perfectly plastic soil models, to correctly link the changes in soil strength with the current effective stress state during analysis. To overcome this problem, effective stress constitutive models should be used for dissipation analysis subsequent to penetration.

Based on a coupled cavity expansion analysis, this paper describes the results of the effects of piezocone penetration at different rates on clays. The penetration process was simplified by the assumption of axial symmetry and plane strain conditions, allowing the piezocone to be modelled as the expansion of a cylindrical cavity. The expansion represents the soil deformation occurring between the tip of the piezocone and the shoulder. This simplification allowed the cone penetration velocity to be linked to the cavity expansion rate, and the predicted pore pressure at the cavity wall to be linked to the dynamic pore pressure measurement at the cone shoulder (u_2). The cavity expansion finite element analysis used the *modified cam* clay constitutive model. Concurrently with penetration, any generated excess pore pressure was

allowed to dissipate. Changes in stresses and pore pressure distributions were assessed for different rate of penetration. Limiting values of excess pore pressure were achieved after a certain rate, which may be used to define the transition from partially drained to fully undrained penetration conditions. Based on a new technique of speed-varying penetration tests [10,11], methods for determining the coefficient of horizontal consolidation are discussed.

To conclude, a comparison is made between centrifuge piezocone tests at different penetration rates and the theoretical analyses shown herein. It is shown that the coefficient of horizontal consolidation relevant to the piezocone dissipation problem, which is analogous to pile set-up, may be estimated from the velocity-dependent change in resistance associated with the transition from undrained to drained behaviour, as well as in the more conventional manner from the subsequent dissipation curve.

CAVITY EXPANSION—FINITE ELEMENT APPROACH

To analyse the effect of penetration rate on the changes of stress and pore pressure distributions in soils, a computer code including a coupled-consolidation formulation was used. This code, referred to as *CAMFE*, was firstly developed at University of Cambridge, U.K., by Prof. Carter [12], whilst the latest versions have been developed at the University of Sydney, Australia [13]. *CAMFE* has previously been used to simulate the expansion of a cylindrical cavity in a saturated two-phase soil (e.g. References [9,14]). The coupled-finite-element formulation is based on the response of the saturated soil element to an applied stress, which is coupled to the Darcy flow of pore fluid through the soil. Details of the numerical formulation, based on the work of Small *et al.* [15], are given by Carter *et al.* [14].

Taking advantage of this formulation, the degree of drainage can be investigated through the variation of either the model permeability or penetration rate. By fixing the penetration rate at 20 mm/s, Abu-Farsakh *et al.* [16] investigated the effect of soil permeability on the computed excess pore pressure during cone penetration. A similar approach was also adopted by Rangeard *et al.* [17] when analysing drainage conditions during pressuremeter tests. In contrast, this paper studies the degree of drainage by imposing a rate of cavity expansion, so that at each time increment dt, the cavity radius r_0 is increased dr_0 in a strain-controlled analysis. Undrained to partially or fully drained condition during the simulation of piezocone penetration is therefore possible by adopting a stepwise finite element approach. If an undrained or a fully drained simulation is needed, then the expansion rate applied relatively to the soil permeability should be sufficiently fast or slow, respectively.

The rate of cavity expansion is related to the penetration rate by the apex angle of the cone. Figure 1(a) shows that, for a vertical penetration rate of v_v, the soil element in contact with a frictionless cone tip surface displaces radially at a constant speed equal to $v_{r0} = v_v \tan\alpha$, where v_{r0} is the rate of cylindrical cavity expansion and α is half of the cone apex angle. For the standard penetration rate of 20 mm/s, the corresponding rate of cylindrical cavity expansion is about 11.5 mm/s over one cone tip length, if a standard 60°-apex angle cone is used. This approach, however, does not account for the axial soil deformation, which accumulates during the steady penetration. The axial strains below the cone tip are a function of the soil strength and the cone angle. For the standard 60°-apex angle cone, for example, during undrained penetration, significant compressive axial strain accumulates ahead of the penetrometer [2,18]. Conversely, a very sharp cone angle mainly displaces the surrounding soil elements in the radial

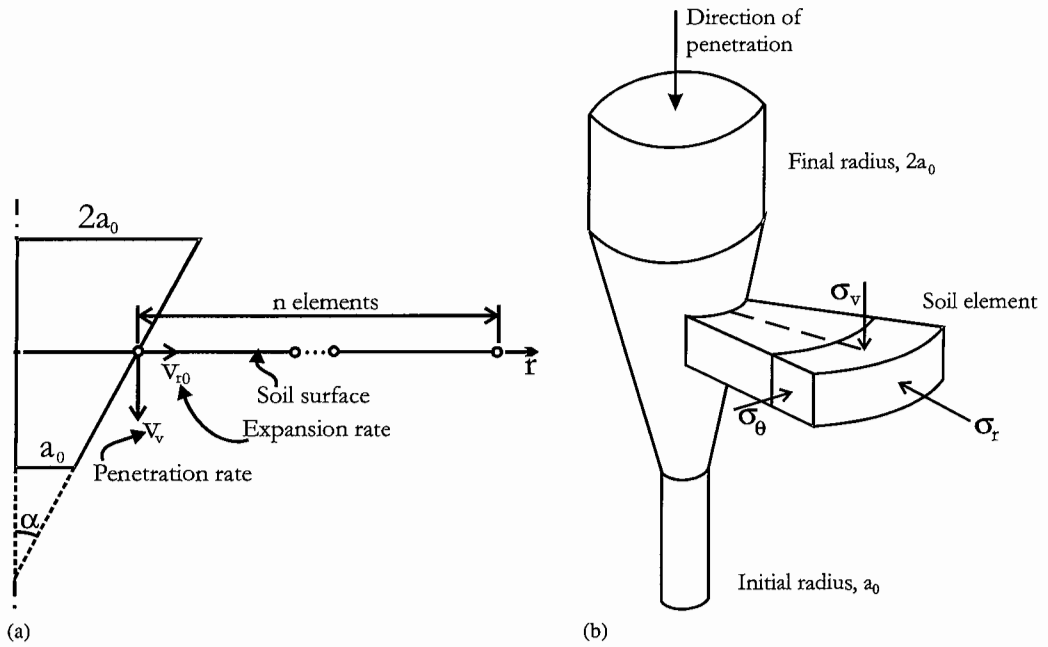

Figure 1. Simulation of the penetration process.

direction. The chosen approach is therefore correct for low values of α, but may introduce an error for higher α values. The simplicity of this model for the penetration process must be weighed against the possible error due to the assumption of wholly radial soil movement.

In a penetration analysis by the cavity expansion approach, plane strain conditions are assumed. The soil is hence considered as a surface of unit thickness in the axial direction. The one-dimensional finite element mesh used in this analysis consisted of 199 nodes, where the ratio of co-ordinates for adjacent nodes was taken as 1.025. Hence, the ratio of the outer boundary of the soil to the penetrometer radius was 76.7. Also, the cavity boundary was considered impervious, while zero excess pore pressure was maintained at all times at the outside mesh boundary.

Singularity of circumferential strain as the cavity is first created is avoided by considering the expansion of a pre-existing cavity of initial radius equal to a_0, to a final cavity of radius a_f [14]. Since cavity expansion is from a finite initial radius, it is necessary to push from a_0 to beyond the radius of the penetrometer r_0, so that the soil that was originally inside a_0 can end up at r_0. To match the stress field, Carter *et al.* [14] suggested a relation between r_0 and a_f found simply by considering constant volume radial movement. The area inside a_0 is soil that must be pushed away to outside the cone radius r_0, to the final cavity radius a_f. So, $\pi a_0^2 = \pi a_f^2 - \pi r_0^2$. If (for convenience) $a_f/a_0 = 2$, then $r_0 = a_0\sqrt{3}$ [14]. The penetration process of a cone penetrometer may then be modelled as indicated in Figure 1(b). For a standard cone penetrometer of diameter 35.7 mm, a cavity of 20.6 mm initial diameter is therefore expanded to a final diameter of 41.2 mm.

SOIL MODEL

In this paper, the *modified cam* clay model [19] was adopted for the study of rate effects on penetration in clays. This model, referred to as MCC, is capable of replicating features of normally consolidated and lightly overconsolidated clays, in which penetration rate effects can be observed. It also permits changes in the strength and density of the soil to be assessed during both cavity expansion and subsequent consolidation.

Two distinct sets of soil parameters were used, representing two example clays: kaolin and Boston blue clay (BBC). The choice of simulating kaolin is because of its wide usage in physical modelling, though pure kaolin is a manufactured product. Parameters for kaolin were obtained from Reference [20], while the BBC properties were chosen from Reference [9]. The numerical values of the soil parameters are tabulated in Table I. In addition to these parameters, a full description of the materials for analysis requires specification of the elastic shear modulus G, the soil permeability k, the unit weight of the pore fluid γ_w and the initial ambient stresses, including the *modified cam* clay hardening parameter p'_c [14].

Prior to the simulation of the piezocone penetrations, different starting stress conditions were considered for each material. Due to the high dependency of cone penetration on the *in situ* horizontal stress [21], the initial effective horizontal stress σ'_{r0} was varied in relation to the initial effective vertical stress σ'_{v0}. Following Randolph *et al.* [9], since the ratio of initial effective horizontal to vertical stresses ($K_0 = \sigma'_{r0}/\sigma'_{v0}$) can be estimated using correlations with overconsolidation ratio (OCR), the K_0 values were linked to increasing OCRs (equal to 1, 2, 4, 8 and 32) as follows:

$$K_0 = K_{0nc}\mathrm{OCR}^n \tag{1}$$

where K_{0nc} is the normally compressed coefficient of earth pressure at rest, and n is a constant. Values of K_{0nc} and n equal to 0.69 [22] and 0.401 [23] were taken for kaolin, respectively. The characteristics of BBC were chosen similar to that of Randolph *et al.* [9], allowing verification of the analyses. For this reason, the initial voids ratio e_0 was considered constant before each analysis, and equal to 1.16 in the case of BBC. For kaolin, the chosen initial voids ratio was 1.41. As pointed out by Randolph *et al.* [9], by adopting a unique initial voids ratio, each material had the same initial plane-strain undrained shear strength s_{u0} prior to piezocone penetration.

In the MCC model, the elastic bulk modulus K' is dependent on the current pressure, whilst G is fixed, resulting in conservative elastic behaviour [24]. In reality, G is not constant, but may be expressed by a power function of the applied pressure p' and pre-consolidation pressure p'_c [25,26]. However, in order to allow comparison of the undrained case results with those of Randolph *et al.* [9], G was tied as a proportion to the maximum value of K' (K'_{max}) that was ever

Table I. Independent constitutive parameters.

	Kaolin	Boston blue clay
λ	0.205	0.15
κ	0.044	0.03
e_{cs}	2.14	1.744
M	0.92	1.2

Table II. Numerical analyses and derived parameters.

Case	OCR	K_0	G/s_{u0}	G/σ'_{v0}	G/p'
Kaolin					
A	1	0.69	78	23	33
B	2	0.91	87	46	57
C	4	1.20	96	90	90
D	8	1.59	105	179	145
E	32	2.77	123	705	325
Boston blue clay					
F	1	0.55	74	25	36
G	2	0.7	83	50	63
H	4	1.0	91	101	100
I	8	1.35	100	201	164
J	32	2.75	118	806	372

reached during the history of the soil, i.e.

$$G = \beta K'_{\max} \tag{2}$$

For linear isotropic elastic material, $\beta = 3(1-2\nu')/[2(1+\nu')]$. For the kaolin, a ν' value of 0.25 was assumed, and hence $\beta = 0.6$, whilst $\beta = 0.5$ was used for BBC [9]. It interesting to note that Equation (2) indirectly connects G (and hence the rigidity index $I_r = G/s_{u0}$) to the OCR values, implying that an overconsolidated soil is stiffer in shear than a normally consolidated soil with the same density. However, it may lead to overprediction of excess pore pressures at high OCR soils, as pointed out by Collins and Yu [27].

The permeability of kaolin was estimated as equal to 1.5×10^{-9} m/s by using the power law relationship of Al-Tabbaa [28], which links k with voids ratio e in the range 0.9–2.4. Due to the anisotropic nature of BBC, a k value of 1.7×10^{-9} m/s, corresponding to the horizontal permeability, was found from Reference [8]. For each soil, the permeabilities were held constant at these initial values throughout the analysis. Hence, the consolidation analysis depended on the value of the soil permeability k, which was assumed constant throughout the cavity creation and subsequent dissipation. The advantage of assuming constant values of permeability at any stress condition is that the changes in consolidation characteristics due to penetration rate are linked only to changes in soil strength and stiffness, as captured by the MCC model. The details of the numerical computations are given in Table II.

RESULTS OF ANALYSIS

By varying the penetration rate v_v, undrained to partially or fully drained penetration conditions were simulated through cylindrical cavity expansion. Figure 2 shows expansion curves of excess pore pressure Δu, which was rendered dimensionless by normalization with s_{u0} [9,14,27]. Figure 2(a) shows $\Delta u/s_{u0}$ as a function of the expanding cavity a/a_0 and the penetration rate v_v, for both kaolin and BBC with OCR = 1. When the cavity has doubled in size, $\Delta u/s_{u0}$ has reached

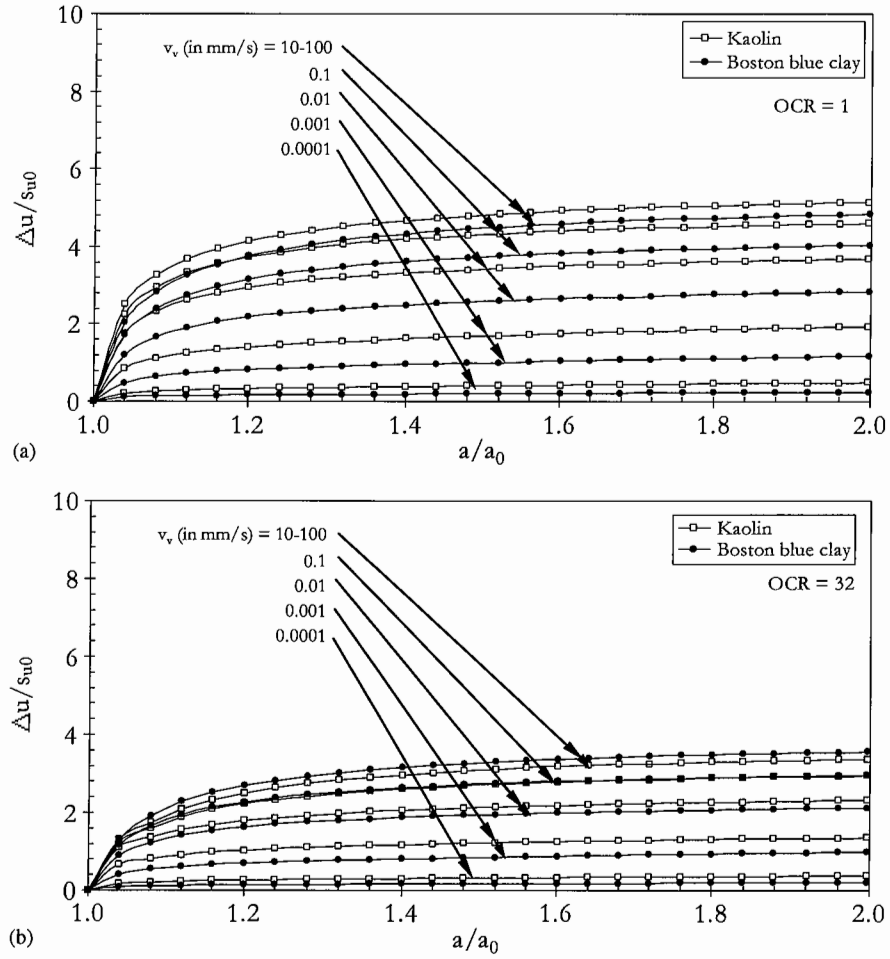

Figure 2. Excess pore pressures generated close to the piezocone face during expansion at different rates.

limiting value. In Figure 2(b), where the initial radial stresses are greater and related to OCR = 32, $\Delta u/s_{u0}$ follows a similar trend but with lower values.

Figure 3 shows the resulting values of $\Delta u/s_{u0}$ obtained after expansion at different penetration rates v_v. It can be observed that, at higher values of OCR, a decrease in $\Delta u/s_{u0}$ is obtained for both soils. This decrease in the $\Delta u/s_{u0}$ values for higher OCR arises since suppressed dilation in high OCR soils creates negative excess pore pressure due to shearing, whereas in low OCR soils the shear-induced Δu is positive. For the soil parameters chosen for analyses, the induced excess pore pressures due to isotropic compression always exceed the shearing components, so the net effect is always a positive excess pore pressure.

As observed in Figure 3, identical values of $\Delta u/s_{u0}$ are developed at 10 and 100 mm/s, indicating that negligible dissipation takes place during penetration. For each soil, this rate of

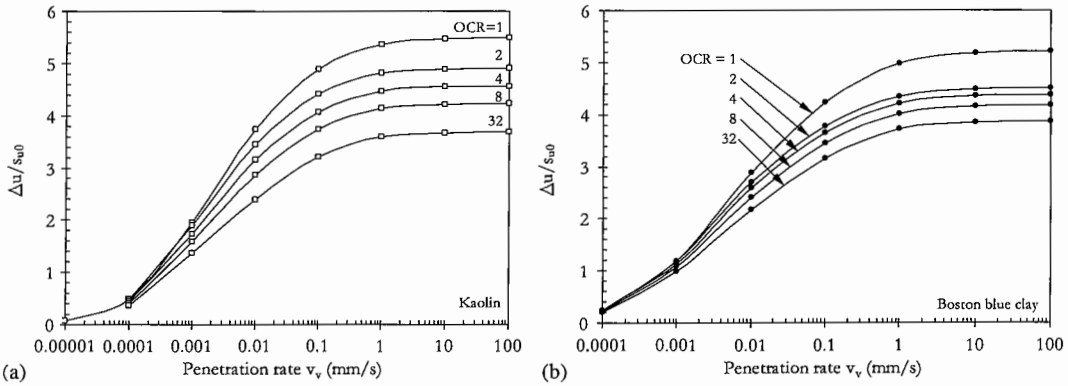

Figure 3. Excess pore pressures close to the piezocone shaft (at $r = 1.15r_0$) after cavity expansion, as a function of penetration rate and OCR.

penetration defines the transition from partially drained to fully undrained penetration conditions. For the kaolin, the $\Delta u/s_{u0}$ values at 10 mm/s penetration rate are only 2% greater than at 1 mm/s, while for BBC this difference is 3.6%. However, there is no difference of Δu between 10 and 100 mm/s penetration rates. The penetration rate which defines the transition between partially drained to fully undrained conditions is therefore in the range of 1–10 mm/s, and is dependent on the consolidation characteristics of the soil.

A higher OCR leads to dilation after failure, counteracting the positive pore pressure generated in response to the increasing total stress. In Figure 3, the overall variation in $\Delta u/s_{u0}$ under undrained conditions is only 3.6–5.6, over a range of OCRs from 1 to 32, for two clays ($M = 0.92$ and 1.2). The parameter M affects the generation of excess pore pressure since it governs the end point of the effective stress path during undrained shear, while the total stress path is governed by the expansion process. As discussed by Randolph *et al.* [9], there is a small influence of both stiffness and stress history of the soil on the excess pore pressure developed under undrained conditions. Therefore, the generation of excess pore pressure is related primarily to the current soil strength, and only marginally influenced by the initial strength and stress history.

An alternative approach to examine the variation of the excess pore pressure (Δu) with OCR is to normalize Δu by σ'_{v0}. Figure 4 shows that the undrained values of $\Delta u/\sigma'_{v0}$ are strongly influenced by OCR. This trend is in agreement with data collected by Lehane [29] from instrumented pile installation in various clays, from which $\Delta u/\sigma'_{v0}$ was found to vary with OCR raised to 0.36–0.5 (for OCR up to 10), depending on the relative depth. However, for higher OCR soils, $\Delta u/\sigma'_{v0}$ tended to reduce, often to negative values, possibly due to soil dilation during shearing along the pile shaft.

Distributions of excess pore pressure and radial stress are plotted in Figures 5 and 6, for kaolin with OCR = 1 and BBC with OCR = 4, respectively (cases A and H of Table II). As shown in Figures 5(a) and 6(a), a higher excess pore pressure is generated immediately after cavity expansion at a higher penetration rate. For comparison, the closed-form solutions for undrained cylindrical cavity creation suggested by Torstensson [30,31] are also plotted. While

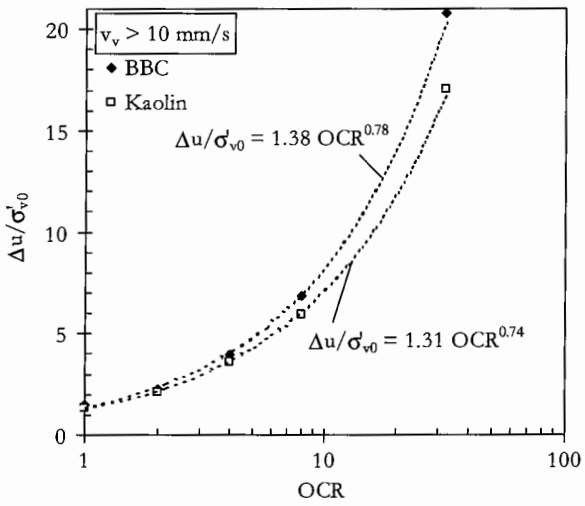

Figure 4. Variation of $\Delta u/\sigma'_{v0}$ with OCR.

good agreement is found between the closed-form solution and the *CAMFE* simulation for BBC ($I_r = 91$), Figure 6(a), the fast penetration distribution of excess pore pressure are greater than the closed-form solution for the normally consolidated kaolin with $I_r = 107$, Figure 5(a).

Higher values of total radial stress are also observed for fast penetration, but the variation with penetration rate is much smaller (Figures 5(b) and 6(b)) when compared with the changes in effective stresses immediately after expansion (Figures 5(c) and 6(c)). It should be noted that ambient pore pressures were not included in any plot of total stress. Even though the penetration rate of 0.0001 mm/s is relatively low, the corresponding cavity expansion rate only allows partial consolidation, leading to a normalized excess pore pressure $\Delta u/s_{u0}$ of 0.5 close to the piezocone shaft immediately after expansion.

Figures 7(a) and (b) show the stress states immediately after cavity expansion for soil elements adjacent to the cone tip for the cases shown in Figures 5 and 6, respectively. The Cambridge q–p' space has been normalized by the initial undrained shear strength s_{u0}. Point A is the initial effective stress state for any rate of penetration. For the fastest penetration rate (= 100 mm/s), the effective and total stress paths (not including the ambient pore pressure) during cavity expansion are plotted as curves AB and AY, respectively. The excess pore pressure immediately after expansion is the horizontal distance BY. For all penetration rates, the final effective stress states lie along the critical state line (CSL). The final total stress states are represented by the curves YY'.

The changes in voids ratio with mean effective stress during cavity expansion for soil elements close to the cone face are shown in e–log p' planes (Figure 8), for the cases presented in Figure 7. Only voids ratio changes for three penetration rates are shown; the fastest, intermediate and slowest speeds, respectively. The points AB are only labelled for the case of the fastest penetration rates. The initial voids ratio is indicated by point A. Like the final stress states, all final voids ratios lie along the CSL immediately after cavity expansion. The reduction in voids ratio increases with reducing penetration rate, as drainage and volume change occurs

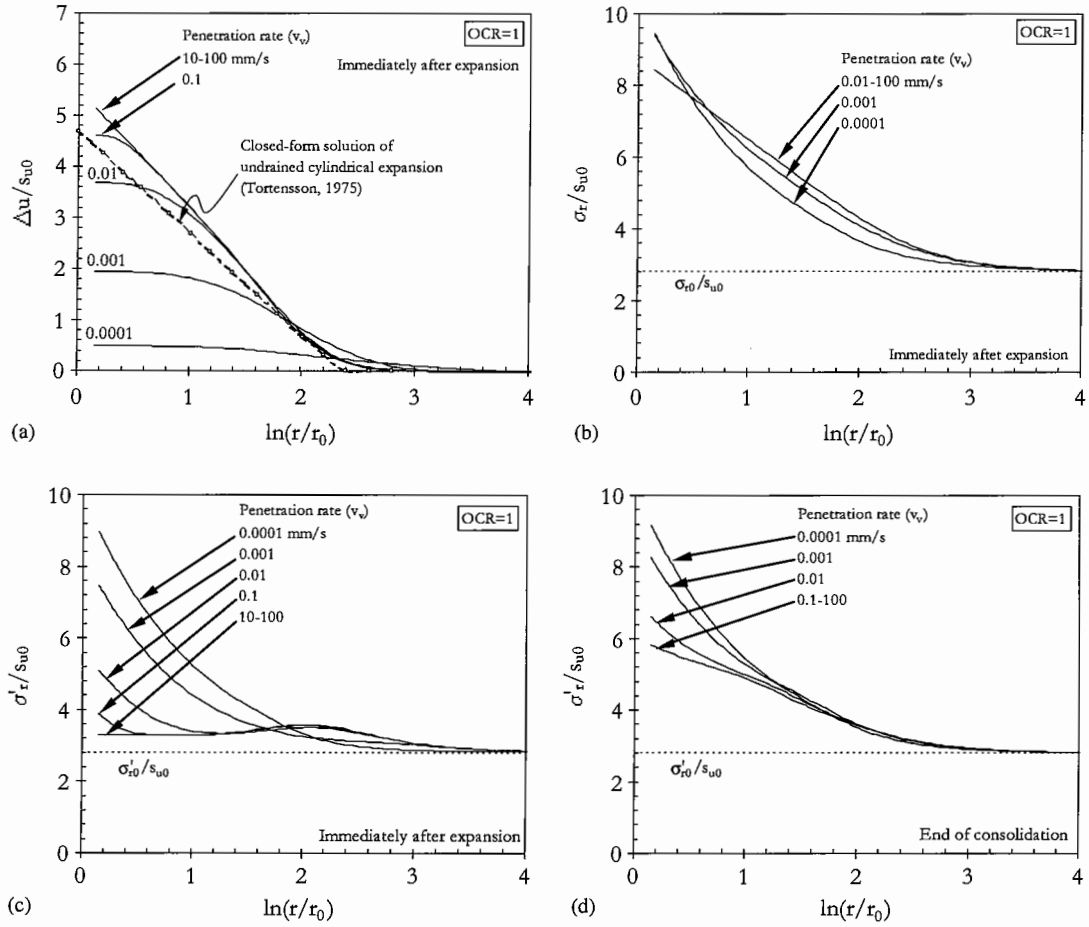

Figure 5. Distributions of excess pore pressure and radial stresses (kaolin, OCR = 1).

concurrently with expansion. In a completely undrained penetration, the initial and final voids ratios of the soil adjacent to the cone face are the same, as is evident for fast penetrations in both clays.

During consolidation (points *B–Z*, Figure 8), the fast tests showed greater contraction, which is to be expected due to the higher excess pore pressure available to drive consolidation. However, this greater contraction during equalization to hydrostatic conditions after undrained penetration left the adjacent soil less consolidated, and hence weaker than after the slower tests.

Figure 9 shows the profiles of voids ratio with radial distance from the penetration axis for cases A and H, considering the fast (100 mm/s) and slow (0.0001 mm/s) cases. For the slow penetration tests, the final voids ratio profiles after dissipation are equal to the profiles of voids ratio immediately after expansion, reflecting the low excess pore pressures after installation, and hence the minimal subsequent consolidation. During undrained penetration, the voids ratio

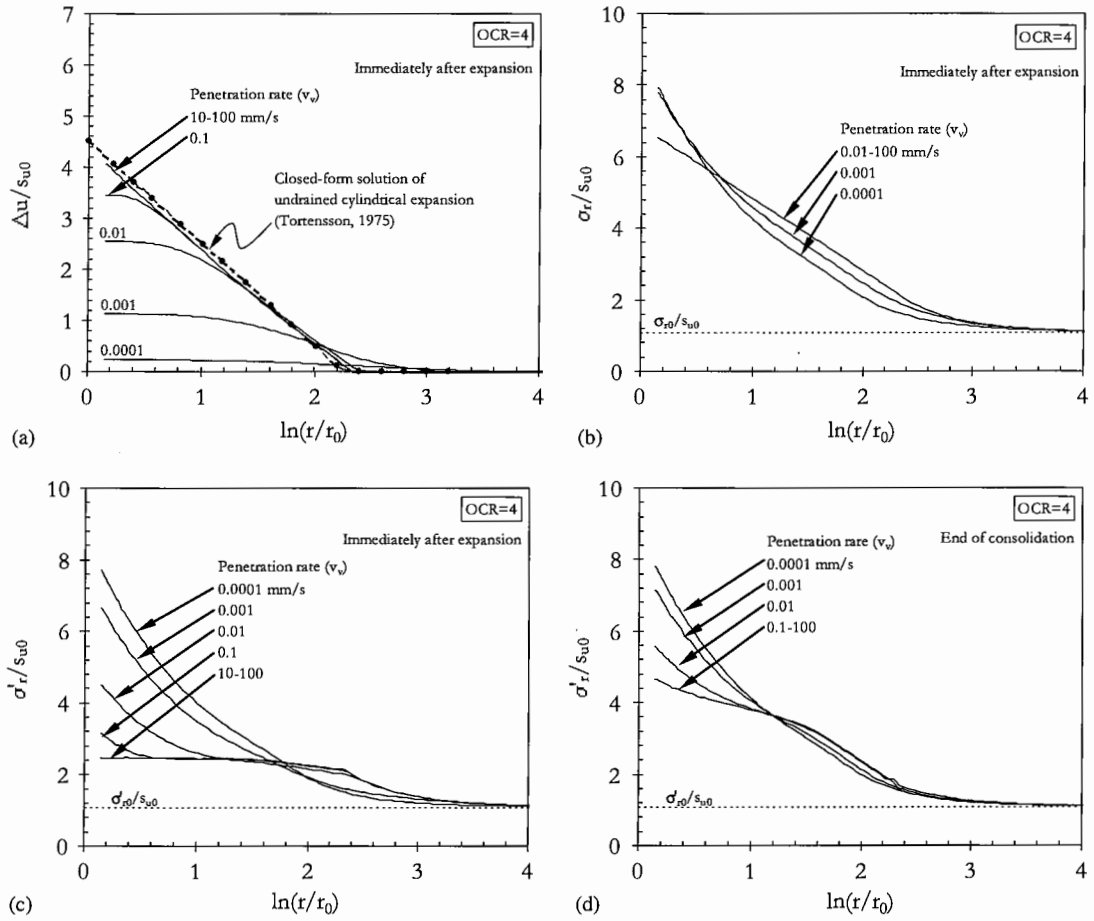

Figure 6. Distributions of excess pore pressure and radial stresses (Boston blue clay, OCR = 4).

profiles immediately after expansion are the same as the initial voids ratio, but during dissipation there is a decrease in voids ratio that reduces with distance from the cone face. This is in agreement with field measurements of changes of moisture contents in the soil adjacent to driven piles immediately after installation [32,33]. Figure 9 also shows that slow penetration has a smaller zone of influence than fast penetration. The cone volume is partly accommodated by consolidation in the near field, rather than wholly by radial displacement at constant volume as is the case for undrained penetration.

Noting that undrained strength increases with decreasing voids ratio, slow penetration leads to stronger soil within $4r_0$ of the cone face and weaker soil beyond, compared to fast penetration. A region of swelling is evident in the far field for BBC with OCR = 4, into which pore fluid is driven as excess pore pressure closer to the cone is dissipated, as noted by Fahey and Goh [34].

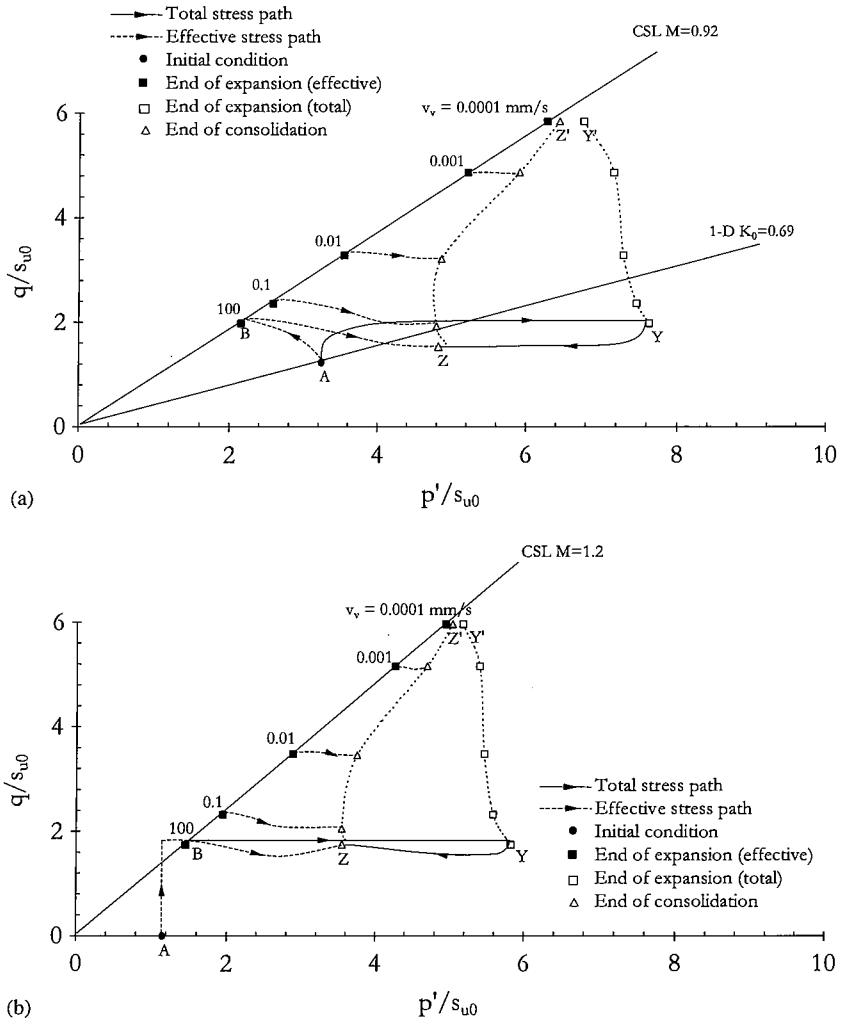

Figure 7. Stress states of adjacent soil close to the cone face during cavity expansion and consolidation: (a) kaolin, OCR = 1; and (b) Boston blue clay, OCR = 4.

NORMALIZATION OF PENETRATION RATE EFFECT

For a coupled analysis, it is intuitive to normalize the penetration rate v_v by a flow parameter, such as the soil permeability k, as follows:

$$\frac{v_v}{k} \tag{3}$$

Based on their finite element simulation, Abu-Farsakh *et al.* [16] evaluated the degree of drainage during penetration using Equation (3). Partially drained penetration was considered to

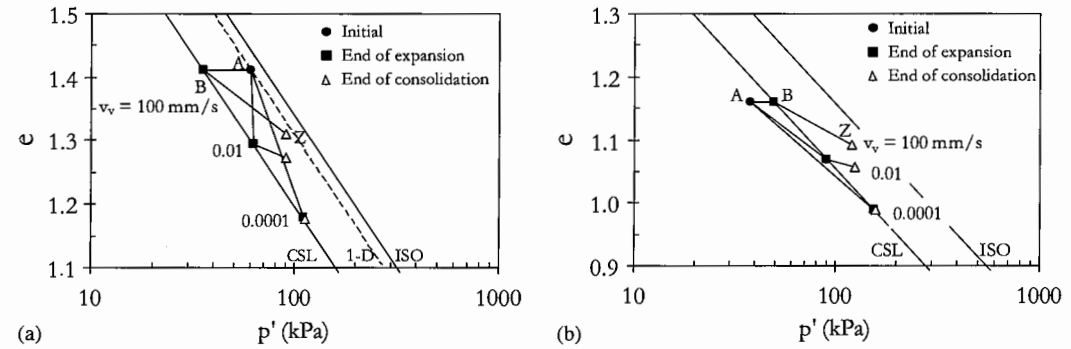

Figure 8. Changes of voids ratio with mean effective stress for soil elements adjacent to the cone face, during cavity expansion and dissipation: (a) kaolin, OCR = 1; and (b) Boston blue clay, OCR = 4.

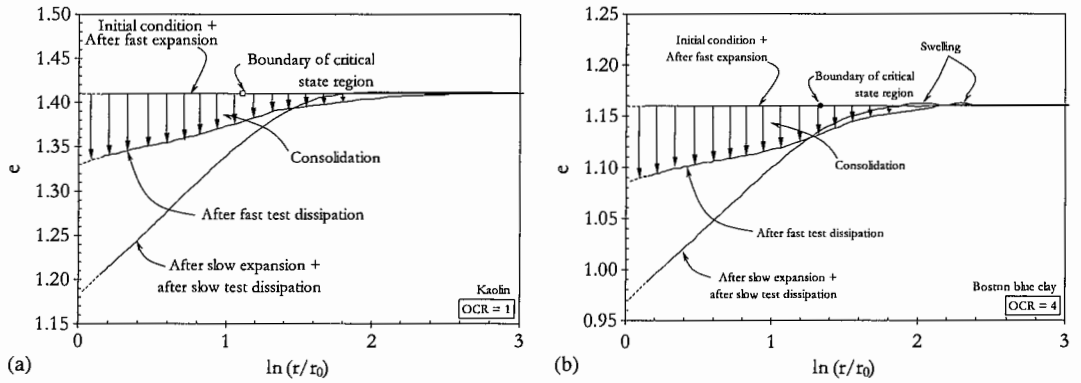

Figure 9. Profiles of voids ratio with radial distance from penetrometer axis, before and immediately after cavity expansion: (a) kaolin, OCR = 1; and (b) Boston blue clay, OCR = 4.

occur for $10^4 < v_v/k < 10^6$, though careful observation of the data implies a greater range for the undrained and drained conditions.

However, the non-dimensional number v_v/k does not adequately account for other factors that govern the consolidation process, namely the soil stiffness and the drainage distance. It may be shown [35] that the penetration of a foundation, or rather in this case a penetrometer [10,11], may be normalized by a non-dimensional velocity number V of the form

$$V = \frac{v_v d}{c_h} \tag{4}$$

where v_v is the penetration rate, d is the diameter of the penetrometer, and c_h is the coefficient of horizontal consolidation. The dimensionless velocity V is equivalent to the ratio of the time for a given fraction of diameter penetration ($= v_v t/d$) to the time for (a given fraction of) consolidation ($= c_h t/d^2$). The c_h values may be calculated as follows:

$$c_h = \frac{k(1+e)\sigma'_r}{\lambda \gamma_w} \tag{5}$$

where k is the soil permeability (assumed constant), e and σ'_r are, respectively, the voids ratio and effective radial stress of the soil adjacent to the cone face immediately after expansion, γ_w is the unit weight of water, and λ is the slope of the CSL in e–$\ln p'$ plane. The selection of λ in Equation (5) links the compressibility of the adjacent soil to the slope of the CSL, which is parallel to the virgin compression line. However, this choice of stiffness value to calculate c_h and V is arbitrary. The soil elements close to the cone are not directly following this path, and soil elements further from the cone lie at a lower stress, so have a lower stiffness.

For normalization of effective radial stresses acting on the cone, a reference radial stress ($\sigma'_{r,ref}$) is conveniently chosen as the limiting effective radial stress after undrained penetration (i.e. at $v_v > 10\,\text{mm/s}$) for each case. The resulting normalizations represent an analytical 'backbone' curve of penetration resistance against rate for a piezocone test, encompassing both drained and undrained penetration (Figure 10). This curve is analogous to the experimentally derived backbone curves for T-bar [10] and model piezocones [11]. There is agreement between the curves for values of V greater than 10, arising from the use of the undrained penetration for reference stresses. However, the curves diverge when V assumes smaller values. This divergence is partly due to the parameters chosen to calculate the c_h values, for which e and σ'_r were taken from the closest element to the cavity immediately after expansion. These parameters, however, assume a different variation with radial distance during slow penetration compared with fast penetration. Hence, the operative coefficient of consolidation at a given distance from the cone, defined as $k/m_v\gamma_w$ (where m_v is the coefficient of volumetric compressibility), varies radially and is dependent on the rate of penetration.

The same normalization is adopted for the maximum excess pore pressure Δu_{max}. For this reason, the limiting excess pore pressures for undrained penetration are taken as reference (Δu_{ref}). The resulting ratios $\Delta u_{max}/\Delta u_{ref}$ are plotted in Figure 11 against the non-dimensional velocity number V. The agreement between the curves for different OCR values, as well as for the two soils, demonstrates the advantage of using V and Δu_{ref} for normalization. These results indicate the proportional reduction in u_2 that would be measured in a decelerating piezocone test for a given value of V, allowing c_h to be deduced. It should be noted that these results rely

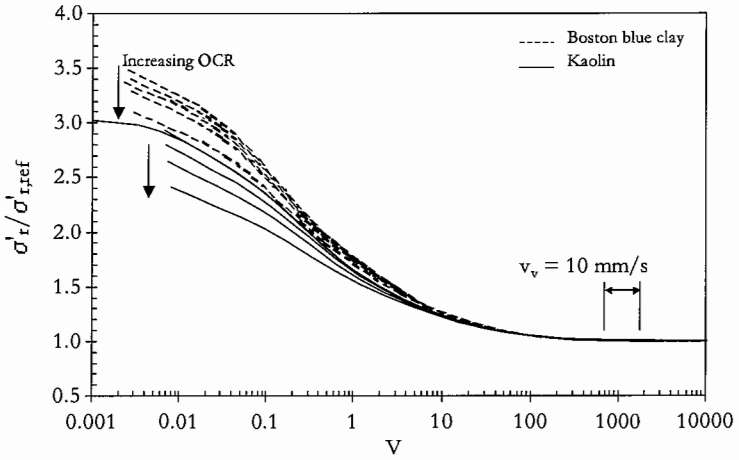

Figure 10. Effect of penetration rate on effective radial stress.

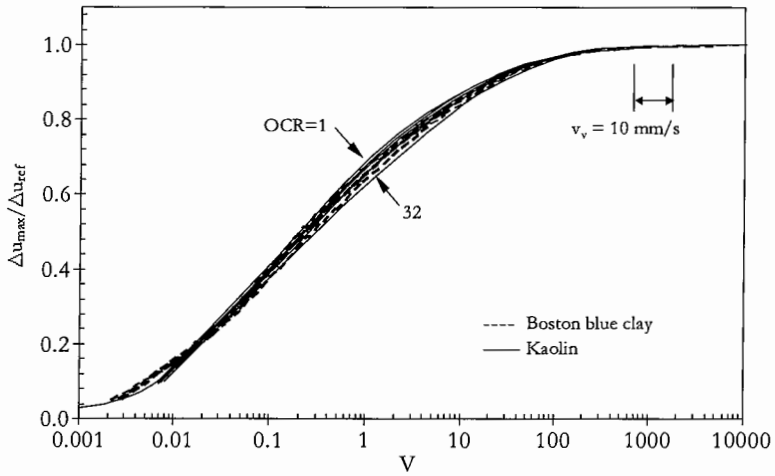

Figure 11. Effect of penetration rate on excess pore pressure.

on the assumptions implicit in this simplified analysis of the penetration process, and the resulting values of c_h correspond to the virgin compression stiffness of the soil at the cone face immediately after cavity expansion (since it is the values of e and σ'_r at the cone face, combined with λ, that are used to calculate the value of c_h used in V).

ESTIMATION OF c_h FROM MULTI-RATE TESTS

It is conventional practice to estimate c_h from a dissipation test for use, for example, in predicting pile set-up. By using the normalized curves linking $\sigma'_r/\sigma'_{r,ref}$ and $\Delta u_{max}/\Delta u_{ref}$ to the dimensionless velocities V, it is alternatively possible to estimate the coefficient of consolidation c_h from the results of two single-rate piezocone tests inserted at different speeds. A value of Δu_{max} can be found at the u_2 position in a slow test, and Δu_{ref} is the undrained excess pore pressure measurement from the u_2 position in a standard (undrained) 20-mm/s piezocone test. Since v_v for the slow test and d are known, c_h can be determined. Alternatively, the corrected cone resistance ratio q_t/q_{ref} can be substituted for $\sigma'_r/\sigma'_{r,ref}$ by assuming that the friction ratio f_s/q_t (and the cone–soil coefficient of friction, σ'_r/f_s) are independent of penetration rate. This approach permits Figure 10 to be used to determine V, and hence c_h.

An alternative suggested by Randolph *et al.* [10,11] is to perform a multi-rate penetration test, where the velocity is successively reduced until the measured resistance or pore pressure has entered sufficiently far into the partially drained region. Then, the results are tied to the respective 'backbone' curve. For example, a piezocone test conducted initially at the standard rate of 20 mm/s, then pushed down 2 diameters at three dimensionless velocities (perhaps around $V=10$, 1 and 0.1) within the partially drained region to identify the 'backbone' curve would take $T^*=\Sigma(2/V)=22.2$. This is comparable to the dimensionless duration of a dissipation test taken to 90% completion, which is typically $T^*=c_h t/d^2\sim 20$. It was shown [11] that, though a greater penetration is required for q_t to become steady, two diameters of

penetration is sufficient for the u_2 measurement to change to a constant value appropriate for the new velocity.

This type of multi-rate penetration test requires precise control of the penetration velocity down to very low speeds, typically in the range of fractions of a mm/s. Rigs capable of these low penetration velocities have been used during research into rate effects, as reviewed in References [4,11] report model piezocone tests at these slow rates. If necessary, a slower cavity expansion rate can be imposed by using a sharper cone angle. This modification to the cone geometry would reduce the errors in this analysis associated with the assumption of wholly radial flow.

DISSIPATION FOLLOWING PENETRATION

After expansion, the analysis was continued to assess the stress changes during excess pore pressure dissipation. As shown in Figures 5(d) and 6(d), the distributions of effective radial stresses (σ'_r) are significantly altered from their initial state at the end of dissipation. The final effective radial stress close to the cone is greatest for the slowest penetration rate. The differences in effective radial stresses for different penetration rates are due to the allowance of partial consolidation during penetration. As observed in Figures 5(b) and 6(b), the total radial stresses immediately after cavity expansion are roughly independent of penetration rate, whilst the effective radial stresses depend on the generation of excess pore pressure, which in turn is dependent on the rate of penetration. During dissipation, there are changes in both total and effective radial stresses [14]: while the effective stresses increase with time, the total stresses decrease, such as observed in field measurements of instrumented piles driven into clays [36,37]. The net result is that drained penetration leads to a higher radial effective stress, lower voids ratio close to the piezocone (or pile), and therefore higher strength in this region, compared with undrained penetration followed by consolidation.

The stress states of elements of soil adjacent to the cone at the end of dissipation are represented by the curves ZZ' in Figure 7. The effective and total stress paths for the soil elements after being subjected to undrained penetrations are also plotted (curves BZ and YZ, respectively). Immediately after expansion, all soil elements adjacent to the cone are on the CSL. As the dissipation takes place, the soil elements close to the cone continue to yield as the stress path moves relatively horizontally in q–p' space. Meanwhile, the more distant soil unloads in shear to stress states inside the current yield locus, as also observed in References [8,9]. This unloading is reflected in the reduction in σ'_{r0}/s_{u0} during consolidation in Figures 5 and 6 at high $\ln(r/r_0)$.

NORMALIZATION OF DISSIPATION CURVES

Analytical solutions of radial consolidation problems usually normalize the decay of pore pressure by a non-dimensional time factor T [38]

$$T = \frac{c_h t}{r_0^2} \tag{6}$$

where c_h is the coefficient of horizontal consolidation, t is the time decay at a specific degree of consolidation, and r_0 is the radius of the penetrometer. As discussed earlier, there is no single

value of c_h to insert in Equation (6) to represent all of the deforming soil, since the soil stiffness varies radially. Throughout the consolidation process, the voids ratios change as the consolidation continues (see Figure 8, curves *BZ*). The slopes of the curves *BZ* in e–$\log p'$ space are different for each previous penetration rate, and none necessarily follows the κ or λ slope of the *modified cam* clay model. For this reason, an operative coefficient of horizontal consolidation for the soil adjacent to the cone during dissipation has been defined as

$$c_h = \frac{k(1 + e_{ave})\sigma'_{r,ave}}{\omega \gamma_w} \tag{7}$$

where e_{ave} and $\sigma'_{r,ave}$ are the average values of e and σ'_r of the soil element adjacent to the cone before and after consolidation, respectively, and ω is the slope of the overall stress path during dissipation in e–$\log p'$ space in Figure 8. After undrained penetration, ω takes a value midway between λ and κ, whereas decreasing the penetration rate the stress paths tend to follow κ, as shown in Figure 13.

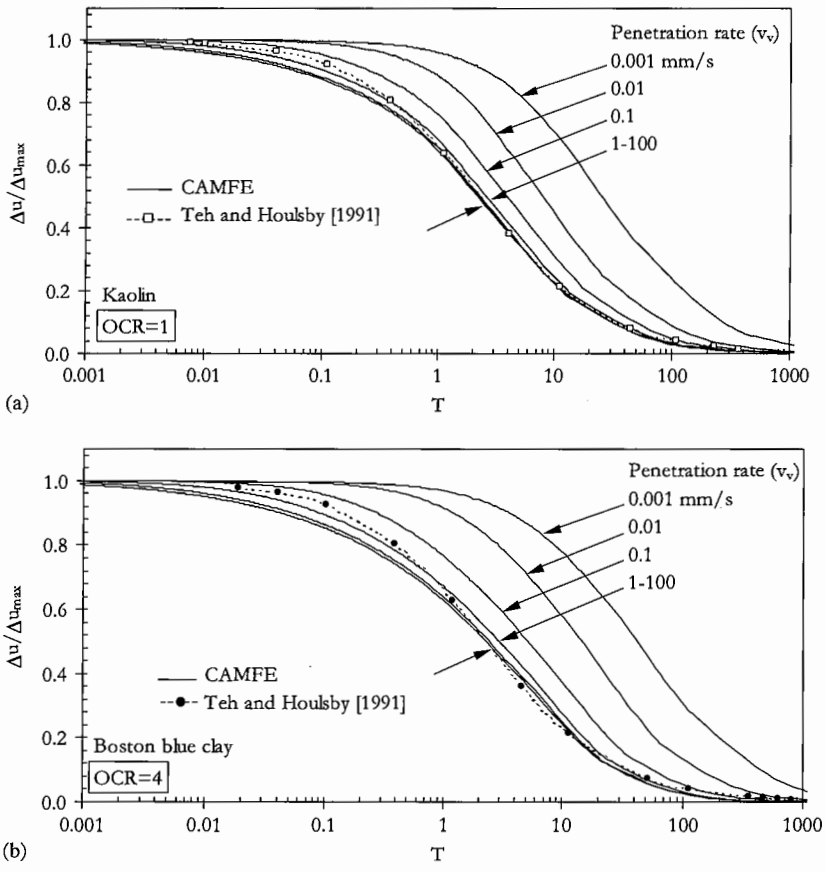

Figure 12. (a) Variation with time of excess pore pressure at $r = 1.15r_0$; and (b) dissipation curves after penetration tests at different rates of penetration at $r = 1.15r_0$.

Figure 12 shows the resulting normalized dissipation curves for the cases A and H of Table II, when the time factor T is calculated using Equation (7). Only monotonic decay takes place after cylindrical cavity expansion since the excess pore pressures are wholly positive and decreasing with radius. The dissipation is faster following the fast penetration tests, since these tests create a higher initial excess pore pressure gradient adjacent to the cone face. The curves are compared with solution given by Teh and Houlsby [2], using the initial rigidity index as given in Table II. The dissipation curves corresponding to the penetration rates in the range 1–100 mm/s agree well with those in Reference [2]. This matches with the observation by Fahey and Goh [34] that c_h values from dissipation tests reflect a soil stiffness given by ω, which is between the unloading and normal compression stiffness, κ and λ, respectively. If c_h is being determined to aid the prediction of set-up around a driven pile, which has the same boundary conditions as piezocone dissipation, this value of c_h is more appropriate than one derived from virgin compression Rowe cell tests, or from the backbone curves presented earlier, which are tied to the virgin compression c_h through the definition of V.

For the slower penetration rates, the normalized dissipation curves are displaced to the right of the curves corresponding to 1–100 mm/s penetration rates by up to an order of magnitude. This variation cannot be wholly attributed to the operative stiffness, ω, which lies within the range λ to κ. The slower dissipation is partly due to the initial distribution of excess pore pressure (Figures 5 and 7). After slow tests, the radial gradient of excess pore pressure at the cone face is very low, so more distant excess pore pressure must dissipate before a hydraulic gradient is present close to the cone. Therefore, c_h estimated from dissipation curves after partially drained penetration will not reflect the same operative soil stiffness as the following undrained penetration if dissipation models such as those in Reference [2] or [6] are used to back-calculate c_h from T.

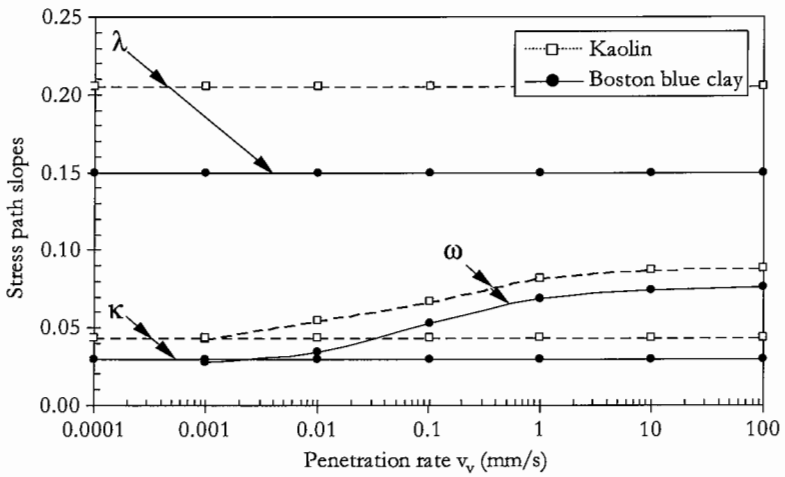

Figure 13. Slope of the overall stress path during dissipation (ω) at $r = 1.15r_0$ vs penetration rate (v_v).

Table III. Kaolin properties [20].

Property	Value
Liquid limit, w_L	61%
Plastic limit, w_P	27%
Soil particle density, G_s	2.6
Angle of internal friction, ϕ'	23°
Slope of critical state line, M	0.92
Critical state voids ratio at 1 kPa, e_{cs}	2.14
Slope of normal consolidation line, λ	0.205
Slope of swelling line, κ	0.044

COMPARISON WITH CENTRIFUGE PIEZOCONE TESTS

In order to evaluate the validity of the partially drained cavity expansion analyses described in this paper, the results are compared to recent centrifuge model penetration tests in normally consolidated kaolin reported in References [11,39]. The programme of penetration tests consisted of nine tests using a 10-mm diameter piezocone in a 650 mm long and 390 mm wide strongbox. The penetration rates ranged from 0.005 to 3 mm/s. In a second kaolin sample, five dissipation tests were performed at different depths after a steady penetration of 1 mm/s. The tests were conducted at a centrifuge acceleration of 100g.

The kaolin samples had an average height of 325 mm, and properties shown in Table III. The coefficient of vertical consolidation (c_v), derived from results of Rowe cell consolidation tests, varied from about 0.032 mm^2/s at the sample surface to 0.127 mm^2/s at an effective vertical stress of 100 kPa. The sample had an average effective unit weight of 6.5 kN/m^3, and a normally consolidated strength ratio s_u/σ'_{v0} of 0.185 was assumed following Stewart [20].

For numerical simulation of these centrifuge tests, the MCC parameters of Table I were used. Since the initial voids ratio of the centrifuge model was similar to the previous numerical simulation of kaolin, the same value of permeability was adopted. As previously, the K_0 value was also assumed to be 0.69 [22]. As will be shown later, the excess pore pressure is correctly estimated when G for the normally consolidated kaolin is calculated as follows [23]:

$$G = 75p' \tag{8}$$

UNDRAINED PIEZOCONE TEST RESULTS

The piezocone test results from the fast penetration tests reported by Randolph and Hope [11] are shown in Figure 14, with numerical analyses conducted at various depths. The plotted experimental resistance is the net corrected cone resistance, $q_{t,net}$ ($=q_t-\sigma_{v0}$). The predicted values of σ'_r, compared with the measured net cone resistance $q_{t,net}$, imply a friction ratio of 7.5% assuming a cone–soil friction coefficient of 0.3; this is slightly higher than is typically measured in normally consolidated clays. The predicted Δu_{max} values compare well with the experimental measurements, indicating that, in this case, the cavity expansion simulation provided a good representation of the penetration process.

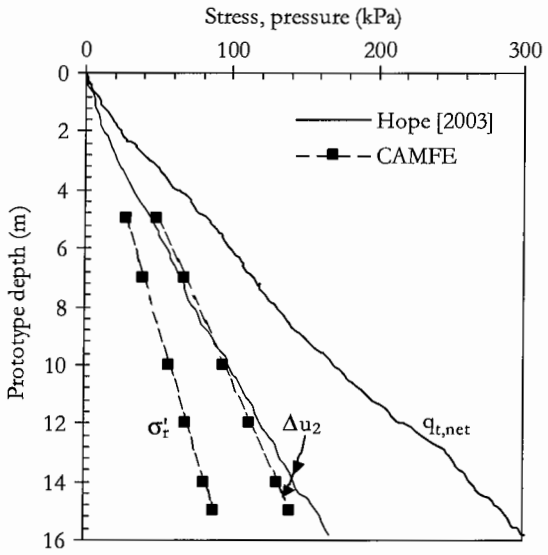

Figure 14. Undrained cavity expansion compared with centrifuge test results from Reference [11].

PARTIALLY DRAINED PIEZOCONE TEST RESULTS

The numerical backbone curves from the finite element analysis are compared with the results from the centrifuge tests in Figure 15. The numerical $\sigma'_r/\sigma'_{r,\mathrm{ref}}-V$ curve is in broad agreement with the $q_{t,\mathrm{net}}/q_{\mathrm{ref}}-V$ curve for the centrifuge model, supporting the assumption that these stress ratios may be compared, and that the friction ratio and cone–soil friction coefficient are independent of rate. The reference stress from the numerical analysis corresponds to the value of σ'_r of a 100 mm/s-penetration rate test, which is fully undrained. The $q_{t,\mathrm{net}}$ values were normalized by a reference cone resistance (q_{ref}) corresponding to the average values of $q_{t,\mathrm{net}}$ for the centrifuge tests at 1 and 3 mm/s penetration rates at the same depth, which are considered undrained. The V values for the centrifuge tests were estimated using the values of c_v from Rowe cell consolidation test increments at the *in situ* vertical effective stress. The numerical analyses were made dimensionless using c_{h} estimated from Equation (5) using λ to represent the soil stiffness and the radial effective stress, σ'_r, after cavity expansion. Since λ is the operative stiffness during a consolidation test, the values of V are comparable, and relate to virgin compression.

Figure 15(b) shows the variation of normalized excess pore pressure with penetration rate. The centrifuge test measurements of $\Delta u_{\max}$ during penetration were normalized by the average values of excess pore pressure of the 1- and 3-mm/s penetration rate tests at the same depth (Δu_{ref}), and the same non-dimensional velocity number V was used as previously. The numerical and centrifuge results match down to a dimensionless velocity of 10 mm/s. However, the numerical simulation shows a gentle decrease of $\Delta u_{\max}/\Delta u_{\mathrm{ref}}$ below this value, while the $\Delta u_{\max}/\Delta u_{\mathrm{ref}}$ from the model piezocone u_2 response drops sharply to zero over only two orders of magnitude of V [11]. The numerical analysis shows a variation in u_2 pore pressure over five orders of magnitude change in V, which is comparable to strain path method solutions for the u_1 position by Baligh (*apud* [40]).

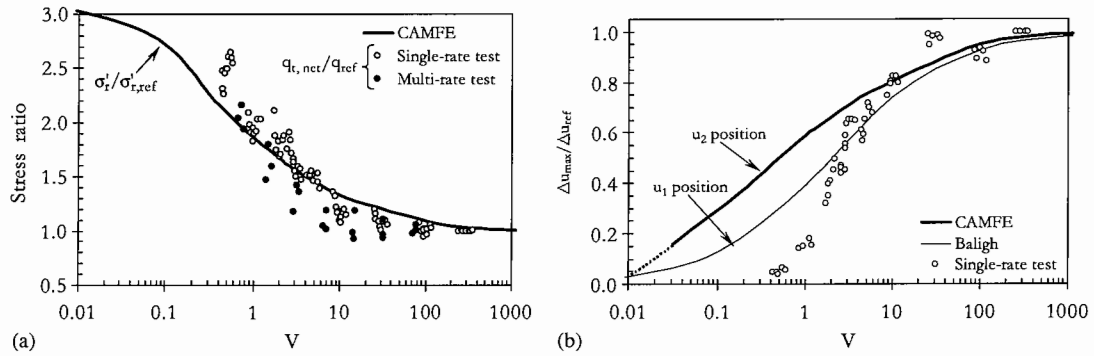

Figure 15. Backbone curves of stress and excess pore pressure compared with centrifuge test results from Reference [11].

In Figure 15, a specific backbone curve for the centrifuge soil model was created using FE, but Figure 10 shows that the backbone curve is relatively unaffected by soil properties. The velocity axis of the backbone curves have been normalized using a c_h applicable to virgin compression (i.e. from Rowe cell tests, or using λ and σ'_r). Therefore, the curves can be used to infer such a value of c_h from an undrained and a partially drained resistance during a multi-speed penetration test. This value of c_h is appropriate for a consolidation-settlement rate calculation since it relates to virgin compression. In order for this value to be useful in predicting pile set-up, it must be established whether the inferred c_h should be modified to simulate the dissipation phase.

It is important to note that there is no particular reason why a virgin compression value of c_h should be used to derive V when normalizing the backbone curve. The stress paths in Figure 8 show that the operative stiffness (and hence c_h) of soil at the cone face depends on the penetration rate itself, and further variations will be present in the radial direction. If a different value of c_h were chosen, for example a value back-analysed from a subsequent dissipation curve, the V axis would be shifted. In this paper, the virgin compression value of c_h has been used to allow comparison with the experimental backbone curves of Randolph and Hope [11], and to produce a backbone curve suitable for back-calculating a c_h relevant to a consolidation-settlement analysis.

DISSIPATION TEST RESULTS

Model dissipation tests were conducted by Hope [39] at four depths after undrained (1 mm/s) penetration (Figure 16). The model test results follow the form of the predicted dissipation curves but with a time lag. In predicting pile set-up, dissipation solutions of the form given in Reference [2] (also see References [6,41]) which assume a constant value of stiffness, and hence c_h are often used. The dissipation approach given in Reference [2] has been used to deduce operative c_h values for the dissipation phase, for comparison with those inferred from the backbone penetration curve.

The deduced values of c_h are shown in Figure 17, assuming the rigidity index I_r of kaolin equal to 322 in the solution in Reference [2]. The I_r value of 322 was estimated using the strength

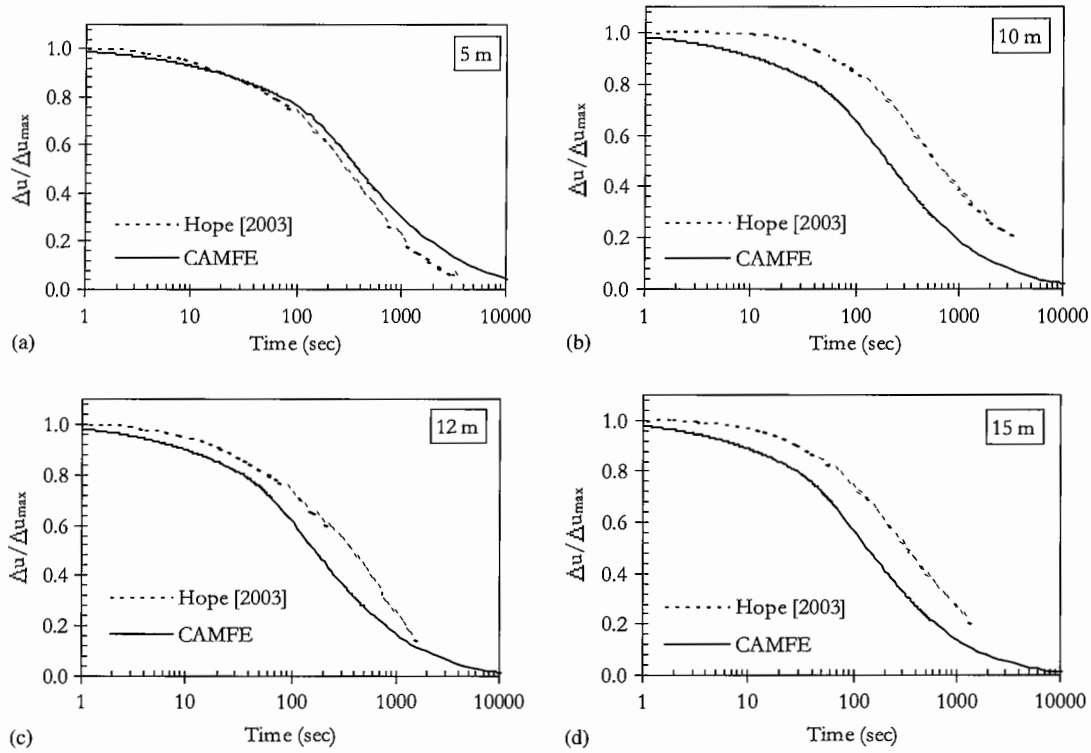

Figure 16. Predicted and measured dissipation tests at various (prototype) depths.

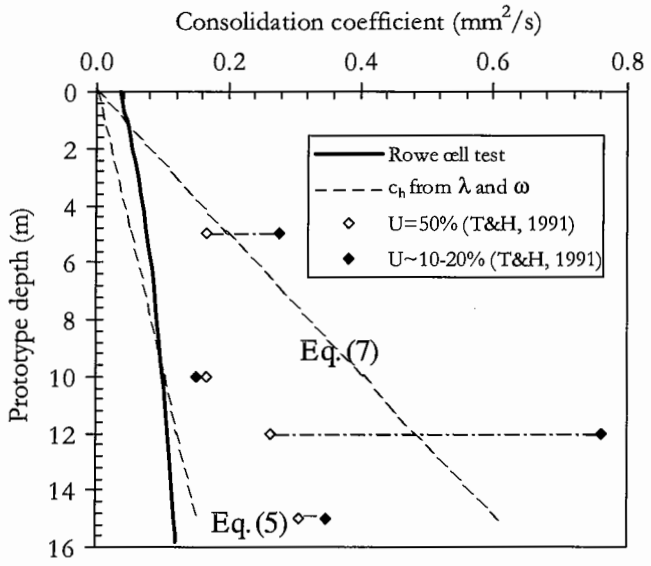

Figure 17. Calculated values of consolidation coefficient, c_h.

ratio s_u/σ'_{v0} of 0.185 and Equation (8). The deduced c_h values are similar to those obtained in Reference [11]. The average values of c_h inferred for the dissipation phase from Reference [2] are greater than the values of c_v from the Rowe cell tests by a factor of 2–2.5. Also, estimations at different degrees of dissipation (at $\Delta u/\Delta u_{max}=0.5$ and approximately at the end of the tests, $\Delta u/\Delta u_{max} \sim 0.1$–$0.2$) give different c_h values. This difficulty was outlined by Battaglio *et al.* [42] from results of field dissipation tests, in which each c_h value corresponded to the stress state of the surrounding soil for the corresponding degree of consolidation.

The profile of c_h with depth deduced using the *in situ* vertical stress and a stiffness of λ from Equation (5) is also shown in Figure 17. This is comparable to the Rowe cell results at about half of the operative c_h during dissipation. The operative value of c_h at the cone face during each dissipation test, found from the analyses shown in Figure 16 using Equation (7), is also shown in Figure 17. This curve shows good agreement with mean values of c_h deduced for the dissipation tests at 5 and 12 m depth, for which the measured and predicted dissipation curves match. Equation (7) is not useful for design since it requires the numerical analyses in order to establish $\sigma'_{r,ave}$, e_{ave}, ω, and hence the operative stiffness at the cone face. However, these results emphasise that the operative c_h back-analysed from constant-stiffness dissipation solutions is typically 2–4 times higher than the value found during virgin compression, and the corresponding stiffness lies between the virgin compression and swelling values.

These observations allow the operative c_h values inferred from the penetration phase to be linked to the operative values during dissipation, or pile equalization and set-up. The penetration backbone curves shown earlier use λ and σ'_r (Equation (5)) to derive a value of c_h for defining V. The numerical dissipation curves after undrained penetration (Figure 12) match the constant-stiffness solution [2] when ω and $\sigma'_{r,ave}$ are used to define c_h (Equation (7)). The result is a difference in operative c_h by a factor of about 3 since ω is lower than λ by a factor of 2 (Figure 13), and $\sigma'_{r,ave}$ exceeds σ'_r by a factor of 1.5.

The centrifuge tests provide comparable experimental evidence for the difference in operative c_h. The centrifuge dissipation curves shown in Figure 16 yield a value of c_h greater by a factor of 2–4 than the Rowe cell values when back-analysed using a constant-stiffness solution. Therefore, values of c_h derived from backbone curves such as Figure 10, in which the velocity is non-dimensionalized using a virgin compression c_h, should be increased by this ratio before being applied to dissipation analyses to estimate pile set-up duration. The use of an unfactored c_h would give a conservatively high set-up duration.

CONCLUSIONS

A set of numerical analyses investigating the effect of penetration rate on piezocone test results in clay has been presented. A coupled cavity expansion finite element method was used to simulate the penetration of a piezocone. The rate of cavity expansion was linked to the penetration rate of the cone and the cone angle, using the assumption that the deformation was wholly radial, and took place only between the cone tip and the cone shoulder.

The soil was modelled using *modified cam* clay. The influence of penetration rate on the stress and pore pressure distributions in soils with different initial conditions was examined. Two soils were modelled, kaolin and Boston blue clay, at OCRs varying from 1 to 32. For a given initial undrained strength, it was shown that the OCR has a significant influence on the generation of

excess pore pressure during undrained expansion, with softer clay (lower OCR) generating greater excess pore pressure.

As the penetration rate reduces, the excess pore pressure at the cone face reduces as consolidation is permitted coincident with penetration. Even for the slowest rate of penetration, 0.0001 mm/s, a normalized excess pore pressure of $\Delta u/s_{u0} = 0.5$ was present at the cone face after installation. The radial distribution of excess pore pressure after slow penetration differs from the undrained case, with a relatively low radial gradient of Δu existing at the cone face. As a result, the dissipation curves after slow penetration lag behind those following fast penetration.

The total stress at the cone face is relatively uninfluenced by the rate of penetration, so the reduced excess pore pressure leads to an increase in the radial effective stress. This can be compared to the increase in cone tip resistance that is seen during slow penetration tests, if it is assumed that the cone friction ratio and coefficient of sleeve friction are unaffected by rate. The radial profiles of post-penetration voids ratio demonstrate that partially drained penetration is permitted partly by volume change in the near field, in addition to radial movement in the far field.

'Backbone' curves of normalized velocity against normalized tip resistance and excess pore pressure capturing the transition from undrained to drained penetration have been derived. The normalized pore pressure backbone curve is unique for both soils over a range of OCRs, whilst the normalized tip resistance shows a small dependency on OCR. The rate of penetration required to observe a change in resistance due to partial drainage is achievable in practice: in a typical offshore soft clay for which $c_h = 0.5\,\text{mm}^2/\text{s}$, a value of $q_{t,\text{net}}/q_{\text{ref}} = 1.5$ would be detected at $V = 2$ (Figure 10), which corresponds to a cone velocity of 1.7 mm/min.

These backbone penetration curves are compared with centrifuge model piezocone tests conducted at varying rates. Dissipation curves are also examined. Whilst good agreement is observed between the curves of normalized velocity and cone resistance, it is interesting that a significant discrepancy exists between the numerical and experimental backbone curves of normalized excess pore pressure.

A complication of analysing drainage during penetration and subsequent dissipation is that the operative coefficient of consolidation is different in each case. The numerical and experimental results suggest that the value of c_h operative during the dissipation phase is 2–4 times higher than the virgin compression value due to changes in the operative soil stiffness. Stress paths followed by soil elements close to the cone face illustrate the different operative stiffnesses during penetration and dissipation. The penetration rate backbone curves have been made non-dimensionless using the virgin compression c_h, following Randolph and Hope [11]. In contrast, when fitting the numerical and experimental dissipation curves to constant-stiffness dissipation solutions such as those in Reference [2], a higher operative c_h is found. The use of multi-rate penetration tests to deduce values of c_h has been discussed, in light of these differences.

NOTATION

a	cavity radius
a_0	initial cavity radius
a_f	final cavity of radius
c_h	coefficient of horizontal consolidation

c_v	coefficient of vertical consolidation
CSL	critical state line
d	penetrometer diameter
$\mathrm{d}r_0$	radius increment
$\mathrm{d}t$	time increment
e	voids ratio
e_0	initial voids ratio
e_{ave}	average voids ratio
e_{cs}	critical state voids ratio
f_s	sleeve friction
G	elastic shear modulus
I_r	rigidity index
ISO	isotropic consolidation line
k	soil permeability
K'	elastic bulk modulus
K'_{max}	maximum elastic bulk modulus
K_0	initial ratio of effective radial to vertical stresses
K_{0nc}	normally consolidated coefficient of earth pressure at rest
M	slope of the critical state line in the q–p' space
OCR	overconsolidation ratio
p'	mean effective stress
p'_c	modified cam clay hardening parameter
q_c	cone resistance
q_{ref}	reference (undrained) cone resistance
q_t	corrected cone resistance
$q_{t,net}$	net corrected cone resistance
r	radial distance from the penetration axis
r_0	penetrometer radius
s_{u0}	initial undrained shear strength
t	time decay
T, T^*	time factor
u	dynamic pore pressure
u_1	dynamic pore pressure at the cone tip
u_2	dynamic pore pressure at the cone shoulder
v_{r0}	rate of cylindrical cavity expansion
v_v	penetration rate
V	dimensionless velocity

Greek letters

α	half of the cone apex angle
γ_w	unit weight of the pore fluid
Δu	excess pore pressure
Δu_{max}	maximum excess pore pressure
Δu_{ref}	reference (undrained) excess pore pressure
κ	slope of the unloading–reloading line in the e–$\ln p'$ plane

λ	slope of the critical state line in the e–$\ln p'$ plane
ν'	Poisson's ratio
σ'_r	effective radial stress
$\sigma'_{r,\mathrm{ave}}$	average value of σ'_r
$\sigma'_{r,\mathrm{ref}}$	reference stress
σ'_{r0}	initial effective radial stress
σ_r	total radial stress
σ_{v0}	initial overburden pressure
ω	slope of the overall stress path during dissipation in the e–$\log p'$ space

ACKNOWLEDGEMENTS

The first author acknowledges the financial support he received from CNPq-Brazil throughout his studies in Cambridge. Also, the support of Giken Seisakusho Ltd. of Kochi, Japan, is gratefully acknowledged.

REFERENCES

1. Yu HS, Mitchell JK. Analysis of cone resistance: review of methods. *Journal of Geotechnical and Geoenvironmental Engineering* 1998; **124**(2):140–149.
2. Teh CI, Houlsby GT. An analytical study of the cone penetration test in clay. *Geotechnique* 1991; **41**(1):17–34.
3. Lu Q, Randolph MF, Hu Y, Bugarski IC. Numerical study of cone penetration in clay. *Geotechnique* 2004; **54**(4):257–267.
4. Lunne T, Robertson PK, Powell JJM. *Cone Penetration Testing in Geotechnical Practice*. Blackie Academic and Professional: London.
5. Burns SE, Mayne PW. Monotonic and dilatory pore pressure decay during piezocone tests in clay. *Canadian Geotechnical Journal* 1998; **35**:1063–1073.
6. Randolph MF, Wroth CP. An analytical solution for the consolidation around a driven pile. *International Journal for Numerical and Analytical Methods in Geomechanics* 1979; **3**(2):217–229.
7. Burns SE, Mayne PW. Analytical cavity expansion-critical state model for piezocone dissipation in fine-grained soils. *Soils and Foundations* 2002; **42**(2):131–137.
8. Baligh MM, Levadoux JN. Pore pressure dissipation after cone penetration. *Report R80-11*, Department of Civil Engineering, Massachusetts Institute of Technology, 1980.
9. Randolph MF, Carter JP, Wroth CP. Driven piles in clay—the effects of installation and subsequent consolidation. *Geotechnique* 1979; **29**(4):361–393.
10. House AR, Oliveira JRMS, Randolph MF. Evaluating the coefficient of consolidation using penetration tests. *International Journal of Physical Modelling in Geotechnics* 2001; **1**(3):17–25.
11. Randolph MF, Hope SN. Effect of cone velocity on cone resistance and excess pore pressure. *Proceedings of the Engineering Practice and Performance of Soft Deposits*, Osaka, 2004; 147–152.
12. Carter JP. CAMFE, a computer program for the analysis of a cylindrical expansion in soil. *Report CUED/C—Soils TR-52*, Engineering Department, Cambridge University, 1978.
13. Carter JP. CAMFE—Version 5.0, a computer program for the analysis of a cylindrical expansion in soil. *Draft of the CAMFE Manual*, Centre for Geotechnical Research, University of Sydney, Australia, 1999.
14. Carter JP, Randolph MF, Wroth CP. Stress and pore pressure changes in clay during and after the expansion of a cylindrical cavity. *International Journal for Numerical and Analytical Methods in Geomechanics* 1979; **3**(4):305–322.
15. Small JC, Booker JR, Davis EH. Elastoplastic consolidation of soil. *International Journal of Solids and Structures* 1976; **12**(6):431–488.
16. Abu-Farsakh M, Tumay M, Voyiadjis G. Numerical parametric study of piezocone penetration test in clays. *International Journal of Geomechanics* (ASCE) 2003; **3**(2):170–181.
17. Rangeard D, Zentar R, Hicher PY, Moulin G. Permeability effect on pressuremeter test results. *Proceedings of the 8th International Symposium on Numerical Models in Geomechanics* (*NUMOG VIII*), Rome, 2002; 619–625.
18. Baligh MM. Undrained deep penetration, I: shear stresses. *Geotechnique* 1986; **36**(4):471–485.

19. Roscoe KH, Burland JB. On the generalised stress–strain behaviour of 'wet' clay. In *Engineering Plasticity*, Heyman J, Leckie FA (eds). Cambridge University Press: Cambridge, 1968; 535–609.
20. Stewart DP. Lateral loading of piled bridge abutments due to embakment construction. *Ph.D. Thesis*, University of Western Australia, 1992.
21. Houlsby GT, Hitchman R. Calibration chamber tests of a cone penetrometer in sand. *Geotechnique* 1988; **38**(1): 39–44.
22. Clegg DP. Model piles in stiff clay. *Ph.D. Thesis*, Cambridge University, 1981.
23. Almeida MSS. Stage constructed embankments on soft clays. *Ph.D. Thesis*, Cambridge University, 1984.
24. Zytynski M, Randolph MF, Nova R, Wroth CP. On modelling the unloading–reloading behaviour of soils. *International Journal for Numerical and Analytical Methods in Geomechanics* 1978; **2**(1):87–93.
25. Houlsby GT, Wroth CP. The variation of the shear modulus of a clay with pressure and overconsolidation ratio. *Soils and Foundations* 1991; **31**(3):138–143.
26. Viggiani G, Atkinson JH. Stiffness of fine-grained soil at very small strains. *Geotechnique* 1995; **45**(2):249–265.
27. Collins IF, Yu HS. Undrained cavity expansion in critical state soils. *International Journal for Numerical and Analytical Methods in Geomechanics* 1996; **20**(7):459–516.
28. Al-Tabbaa A. Permeability and stress–strain response of speswhite kaolin. *Ph.D. Thesis*, Cambridge University, 1987.
29. Lehane BM. Experimental investigations of pile behaviour using instrumented field piles. *Ph.D. Thesis*, University of London, 1992.
30. Torstensson BA. Pore pressure sounding instrument. *Proceedings of the ASCE Specialty Conference on In Situ Measurements of Soil Properties* (*ISMOSP*), Raleigh, vol. 2, 1975; 48–54.
31. Torstensson BA. The pore pressure probe. *Geoteknikkdagen*, Paper 34, Oslo, 1977; 1–15.
32. Cummings AE, Kerkhoff GO, Peck RB. Effect of driving piles into soft clays. *Transactions of the American Society of Civil Engineers* 1950; **115**:275–350.
33. Rutledge PC. Discussion on effect of driving piles into soft clay. *Transactions of the American Society of Civil Engineers* 1950; **115**:301–304.
34. Fahey M, Goh AL. A comparison of pressuremeter and piezocone methods of determining the coefficient of consolidation. *Proceedings of the 4th International Symposium on the Pressuremeter and its New Avenues*, Quebec, 1995; 153–160.
35. Finnie I, Randolph MF. Punch-through and liquefaction induced failure of shallow foundations on calcareous sediments. *Proceedings of the International Conference on Behaviour of Offshore Structures* (*BOSS'94*), Boston, 1994; 217–230.
36. Lehane BM, Jardine RJ. Displacement-pile behaviour in a soft marine clay. *Canadian Geotechnical Journal* 1994; **31**(2):181–191.
37. Dias CRR. Behaviour of an instrumented driven pile in soft clay. *D.Sc. Thesis*, COPPE, Federal University of Rio de Janeiro, 1988 (in Portuguese).
38. Soderberg LO. Consolidation theory applied to foundation pile time effects. *Geotechnique* 1962; **12**:217–225.
39. Hope SN. The effect of consolidation on the bearing resistance of penetrometers. *Honours Project Report*, School of Civil and Resource Engineering, Centre of Offshore Foundation Systems, University of Western Australia, 2003.
40. Hight DW, Leroueil S. Characterisation of soils for engineering purposes. In *Characterisation and Engineering Properties of Natural Soils*, Tan TS, Phoon KK, Hight DW, Leroueil S (eds), vol. 1. Balkema: Rotterdam, 255–360.
41. Whittle AJ, Aubeny CP. Effects of installation disturbance on interpretation of in situ tests in clay. *Proceedings of the Predictive Soil Mechanics, Wroth Memorial Symposium*, Oxford, 1992.
42. Battaglio M, Jamiolkowski M, Lancellotta R, Maniscalco R. Piezometer probe test in cohesive deposits. *Proceedings of the Cone Penetration Testing and Experience*, ASCE, New York, 1981; 264–302.

